International Journal of Technology

http://ijtech.eng.ui.ac.id

Research Article

Synthesis, Characterization, and Conductivity Evaluation of CuNP-rGO-PANI Nanocomposites for Printed Sensors

Priska Wisudawaty [1,2], Endang Warsiki [3,*], Sugiarto [3], Taufik Djatna [3]

[1]*Postgraduate Program in Agroindustrial Engineering, IPB University, Bogor 16680, Indonesia*
[2]*Industrial Engineering Study Program, Universitas Teknologi Bandung, Bandung 40235, Indonesia*
[3]*Department of Agroindustrial Technology, Faculty of Agricultural Engineering and Technology, IPB University, Bogor 16680, Indonesia*
[*]*Corresponding author: endangwarsiki@apps.ipb.ac.id; Tel.:* +61-25-18621974

Abstract: Nanocomposites composed of copper nanoparticles (CuNP), reduced graphene oxide (rGO), and polyaniline (PANI) have garnered considerable attention due to their potential as conductive materials for printed sensor applications. This study aims to synthesise CuNP-rGO-PANI nanocomposites through a chemical reduction method and examines their structural, morphological, and electrical properties. The synthesis process involves reducing graphene oxide (GO) using sodium borohydride ($NaBH_4$), followed by the incorporation of CuNP and PANI through in-situ polymerization. The synthesized nanocomposites were characterized using Fourier-transform infrared (FTIR) spectroscopy, Raman spectroscopy, and scanning electron microscopy (SEM) to verify their chemical composition and morphological structure. Additionally, the electrical conductivity of the CuNP-rGO-PANI nanocomposites was evaluated to determine their feasibility for printed sensor applications. Raman spectroscopy results reveal that the incorporation of Cu nanoparticles increases the ID/IG ratio, indicating a rise in structural defects within rGO. SEM analysis determined that the average particle size of the CuNP-rGO-PANI nanocomposite is approximately 11.48 nm. FTIR characterization further demonstrates that the addition of CuNPs alters the oxidation state of both PANI and reduced graphene oxide. Among the tested substrates, polyethylene terephthalate (PET) exhibited the highest conductivity of 1.486 S/cm, which is attributed to an optimal coating thickness and uniform particle distribution.

Keywords: Conductive inks; Copper nanocomposite; CuNP-rGO-PANI; Graphene; Sensors

1. Introduction

The advancement of nanomaterial-based sensor technology has become a significant area of interest within functional materials research, primarily due to the necessity for more efficient,

This work was supported by the (1) Pusat Pembiayaan dan Asesmen Pendidikan Tinggi (Center for Higher Education Funding and Assessment)-PPAPT Ministry of Higher Education, Science, and Technology of Republic Indonesia, and (2) Education Fund Management Institution (LPDP), Ministry of Finance Indonesia. Fund Project Number: 1985/J5.2.3./BPI.06/10/2021.

https://doi.org/xx/ijtech.xx
Received date; Revised date; Accepted date

flexible, and integrated sensor devices with printed electronic systems. In this context, graphene-based nanocomposites, such as reduced graphene oxide (rGO), have garnered considerable attention due to their exceptional electrical, thermal, and mechanical properties. Nevertheless, structural modification is necessary to enhance these materials' functionality by incorporating alternative conductive materials, including metal nanoparticles (MNPs) and conductive polymers.

Nanocomposites represent a significant advancement in materials science, offering the unique ability to integrate the exceptional attributes of diverse materials into a unified and synergistic system. Various conductive materials have been developed for use in printed electronics in recent years. However, some inherent limitations restrict their applications. For instance, polymer-based materials exhibit poor conductivity, while pure metal materials, including Au, Ag, Pt, and Cu (Park et al. 2007; Nur et al. 2002) demonstrate excellent conductivity but are prohibitively expensive for mass production due to their tendency to oxidize and exhibit poor sensitivity (Junervin, Djatna and Fahma, 2020). Carbon-based nanomaterials, including carbon-based nanofibers, activated carbon, and graphene, have been shown to exhibit optimized conductivity, a large surface area, and high anti-corrosion ability (Trisnadewi et al., 2023; Murdiya et al., 2022; Gao 2017; Qiu et al. 2017; Mohanapriya, Ghosh, and Jha 2016; Wang, Yan, and Fan 2016; Filip, Kasák, and Tkac 2015; B. Q. Li et al. 2015). Graphene possesses distinctive properties, including a high surface area, high chemical stability, rapid electron transfer kinetics, and exceptional electrocatalytic characteristics (Hardi and Rahman, 2020; Kusrini et al., 2019; Xu et al., 2014). Due to these properties, graphene is frequently employed in synthesizing nanocomposites for sensing applications. In order to obtain the maximum physical and chemical characteristics, graphene must be subjected to a reduction process to produce rGO. Reduced graphene oxide (rGO) exhibits high electrical conductivity and a large surface area, facilitating efficient charge transfer and analyte (Fajarani et al., 2024; Yao, 2022; Bhangoji et al., 2021). However, the primary disadvantage of rGO is its tendency to aggregate and revert to a graphite form (Kumar et al., 2018). One potential solution to this challenge is the synthesis of graphene with various noble metals to create layered nanocomposites that enhance electrochemical processes (Mooss et al. 2017; Pandey and Qureshi 2017; R. Li et al. 2017; Kalambate et al. 2015; Shahriary et al. 2015).

Metal-based nanocomposites, such as copper (CuNP) nanoparticles combined with rGO and polyaniline, have emerged as promising candidate materials for this application. The combination of the high conductivity properties of metals with the flexibility and chemical stability of rGO and PANI is anticipated to result in the creation of materials with optimal performance as essential elements in chipless RFID.

CuNPs offer high electrical conductivity at a lower cost, are abundant, possess antimicrobial properties, and demonstrate significant electrochemical activity. Moreover, they can be readily synthesized in a variety of nanoscale forms. Copper is receiving heightened interest for its potential use in sensors, its effectiveness in electrochromic coatings, and its possible use in superconductors, making it a compelling subject for research (Nugrahaningtyas et al., 2025; Wu et al., 2017; Dobrovolný, Ulbrich and Bartůněk, 2016; Mousavi-Kamazani, Zarghami and Salavati-Niasari, 2016; Martinez-Lombardia et al., 2014; Reddy et al., 2014).

Polyaniline (PANI) is a conductive polymer that, when doped, enhances the overall electrical conductivity of the composite. PANI also provides flexibility and processability, which, when coupled with rGO and nanoparticles, results in composites with an optimal balance between conductivity, strength, and stability (Petrovski et al. 2017; Z. F. Li et al. 2014; Y. Liu et al. 2014).

Compared to sensors based on metal oxide materials or carbon nanotubes, which have been widely used commercially, CuNP/rGO/PANI nanocomposites offer potential advantages such as excellent electrical conductivity, outstanding thermal stability, high mechanical strength, and enhanced catalytic or antimicrobial properties (Shishir et al., 2024). This combination makes them

highly suitable for applications in sensors, energy storage devices, coatings, and biomedical fields, where the synergistic performance of the composite is crucial. This is because rGO provides support sites for CuNPs, preventing aggregation and improving their stability. The combination of CuNPs, rGO, and PANI creates a percolation network for efficient charge transport. Additionally, the PANI polymer matrix maintains flexibility, while rGO enhances durability, preventing degradation.

Additionally, CuNP-rGO-PANI nanocomposites demonstrate considerable potential for incorporation into active and intelligent packaging technologies. In the context of active packaging, CuNP has been demonstrated to possess antibacterial properties that can inhibit the growth of microorganisms, thereby extending the product's shelf life. Investigated the potential of chitosan as a biomaterial for ethylene-absorbing active packaging in a related field (Warsiki, 2018). Conversely, the conductive and flexible properties of CuNP-rGO-PANI facilitate the printing of sensors on the packaging surface, which can detect alterations in temperature, humidity, or product quality in real-time, thus enabling the development of innovative packaging. Integrating sensors into the packaging of agro-industrial products offers consumers several significant advantages, including the assurance of freshness and quality. Furthermore, it allows the retail industry to efficiently manage stock and verify product authenticity (Wisudawaty, Djatna and Sugiarto, 2024).

Although various synthesis methods have been developed, such as sol-gel, hydrothermal, and chemical vapor deposition, challenges remain in optimizing the nanocomposite composition ratio and printing techniques to produce high-performance sensors. For instance, different synthesis methods can influence the electrical conductivity and stability of the sensor, while printing techniques such as screen printing can affect the print pattern and sensor reproducibility. The success of this application depends on the development of an ink formulation with optimal viscosity and high conductivity. Consequently, advancements in CuNP-rGO-PANI nanocomposite-based inks present a significant challenge, requiring a comprehensive scientific approach encompassing synthesis, characterization, and material performance evaluation.

From the perspective of research advancements, this study offers a more controlled synthesis method by varying reaction conditions and optimizing reduction techniques to achieve a more uniform distribution of CuNPs within the rGO-PANI matrix. Additionally, it focuses on optimizing printing techniques, particularly by evaluating the effectiveness of screen printing on flexible substrates such as PET, glass, and photo paper which has been rarely discussed in previous studies.

This research aims to develop and characterize CuNP-rGO-PANI nanocomposites, utilize the nanocomposites as conductive inks, and evaluate their conductivity properties for printed sensor technology. Therefore, this research is expected to contribute to the development of more effective, efficient, and sustainable nanocomposite-based printed sensors.

2. Methods

2.1 Synthesis of Graphene Oxide (GO)

The synthesis of GO was conducted using the modified Hummers method, as described by (Liu et al., 2014). 6 g of graphite powder were dissolved in 130 mL of concentrated sulfuric acid (98% H_2SO_4). Subsequently, 4 g of $NaNO_3$ were added and stirred for 4 hours (temperature <20°C) by placing the mixture in an ice bath. After 2 hours of stirring, 8 g of $KMnO_4$ was added to the solution gradually, after which homogenization was conducted for a further 2 hours at a temperature of 35°C. Subsequently, 200 mL of distilled water was incorporated gradually and homogenized for 1 hour. Subsequently, 20 mL of H_2O_2 (30%) was introduced to remove any residual $KMnO_4$.

Subsequently, the mixture was subjected to centrifugation, and 80 mL of HCl was introduced to facilitate the elimination of any residual metal impurities. Subsequently, the pH was neutralized through leaching and the residual SO_4^{2-} ions were minimized. Once a neutral pH was reached, the

mixture was dried for 12 hours at 110°C. Subsequently, the dried graphene oxide (GO) was exfoliated to create graphene oxide sheets. 40 mg of GO was combined with 40 mL of distilled water, stirred for 1 hour to form a homogeneous solution, and subjected to ultrasonication for 120 minutes. The application of ultrasonic waves resulted in the peeling of graphite oxide into GO.

2.2. Reduced Graphene Oxide (rGO)

The graphene oxide (GO) obtained from the ultrasonication process was subjected to a chemical reduction process using sodium borohydride ($NaBH_4$). The reduction process is conducted by introducing $NaBH_4$ to the graphene oxide suspension in a ratio of 9:7 (Sharma et al., 2017), while maintaining vigorous stirring for 10 minutes. Subsequently, the solution was placed in an autoclave at 200°C for 5 hours (Kumar et al., 2018). Following the reduction process, the rGO is subjected to a pH neutralization procedure involving a washing step with running water. Subsequently, the material is transformed into a powder form by drying at a temperature of 110°C.

2.3. Synthesis of CuNP-rGO-PANI Nanocomposites

Aniline polymerization was employed in situ to synthesize the CuNP-rGO-PANI nanocomposites. The process entailed the preparation of 3 distinct solutions. Solution A: 200 mg of rGO were dissolved in 200 mL of water, and the resulting solution was then subjected to sonication for 120 minutes. Solution B: Copper sulfate pentahydrate ($CuSO_4 \cdot 5H_2O$) was dissolved in distilled water and stirred for 20 minutes to create a 0.01 M solution. In a separate step, a solution of 0.02 M ascorbic acid was prepared in distilled water. Subsequently, the copper sulfate solution was added to the ascorbic acid solution, and stirring was maintained throughout. To adjust the pH, 1 M NaOH in distilled water was added. Following a 30 minute stirring period, 0.1 M $NaBH_4$ in distilled water was introduced gradually with continuous stirring. After 15 minutes, the initial blue mixture underwent a colour change, becoming reddish-brown. Solution C was prepared by dissolving 2 mL of aniline in 60 mL of distilled water, then adding 0.5 mL of concentrated HCl and homogenization for 30 minutes.

The CuNP-rGO-PANI nanocomposite was prepared: Solutions A and B were combined and stirred for 1 hour. Solution C was then added and stirred for another 20 minutes. Subsequently, 40 mL of an aqueous solution containing 1 g of ammonium persulfate (APS) was added gradually. The mixture was homogenized and allowed to polymerize for 12 hours. The precipitate obtained was washed under running water. To obtain the nanocomposite in powder form, the precipitate was dried at 70°C.

2.4. Sample Characterisation

A variety of analytical techniques were employed to characterize the processed samples. Raman spectroscopy is a technique employed for the identification of molecules, the analysis of chemical structures, and the investigation of molecular interactions within a given sample. This method is based on inelastic light scattering, also known as Raman scattering, in which light incident on a sample undergoes a frequency shift due to interaction with the sample's molecular vibrations. The sample's morphology was examined using a scanning electron microscope (SEM), and any complex groups were identified using a Fourier transform infrared (FTIR) spectrometer.

2.5. Conductive Ink Preparation and Sensor Printing

The conductive ink was prepared by combining a conductive material, specifically a CuNP-rGO-PANI nanocomposite, with a epoxy resin and dispersing the mixture in distilled water and ethanol. This resulted in a paste-like ink, subsequently utilized in fabricating sensors. The sensor was printed using the screen printing method with a T90 mesh screen. Patterns in the form of lines with dimensions of 1 × 2 cm were printed on paper and transferred to a screen previously coated with

emulsion. Subsequently, the screen is subjected to solar drying for approximately 20 seconds and rinsed with water until the requisite pattern is formed. The conductive ink is then applied to the screen and printed on Polyethylene Terephthalate (PET) (Liu et al., 2021), glass, and paper, which were prepared previously (Figure 1). Once the printing process is complete, the printed material must be cured using an oven set to 100°C for 12 minutes.

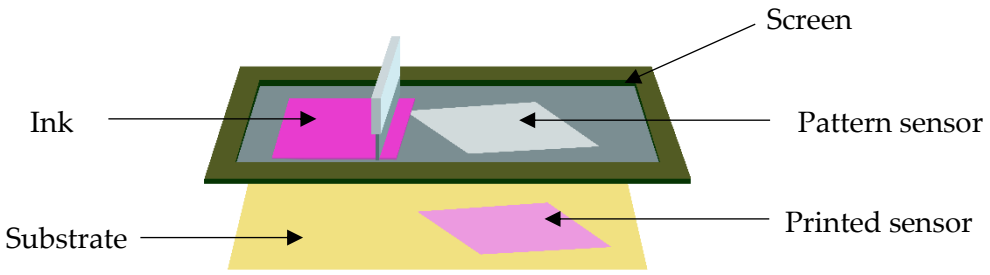

Figure 1 Illustration of screen printing method

2.6. Sensor Characterization

The previously manufactured film-shaped sensor is subjected to electrical conductivity measurement via the 4-point probe method, employing a multimeter and a 12V current source. To calculate the electrical conductivity, equations 1 and 2 are used (Istuk et al., 2023):

$$\rho = \frac{V}{I} + \frac{d}{s} + C' \quad (1)$$

$$\sigma = \frac{1}{\rho} \quad (2)$$

Description:
ϱ = resistivity (Ω)
V = electric potential difference (V)
I = electric current (A)
d= sample surface width (cm)
s = distance between probes (cm)
C' = correction factor
σ = electrical conductivity (S/cm)

3. Results and Discussion

3.1. Synthesis Results of CuNP-rGO-PANI Nanocomposites

Graphene oxide is produced from graphite base material through the Hummers oxidation method (Liu et al., 2014). The oxidation process entails the utilization of potent acids, which facilitate the disruption of inter-carbon bonds and the spacing of graphene sheets. Subsequently, exfoliation is conducted via ultrasonication, which results in the complete disruption of the inter-sheet bonds. To enhance graphene's chemical and physical attributes, specific oxide groups must be eliminated through a reduction process, which can be accomplished either through chemical means or hydrothermal methods, resulting in reduced rGO. Nevertheless, the primary disadvantage of rGO is its proclivity to agglomerate and revert to the graphitic form (Kumar et al., 2018). Incorporating copper (Cu) nanoparticles via in situ polymerization of aniline is designed to function as nanoscale spacers, increasing the distance between graphene sheets (Tien et al., 2011) and thus preventing their aggregation. Figure 2 illustrates the synthesis process of CuNP-rGO-PANI nanocomposites.

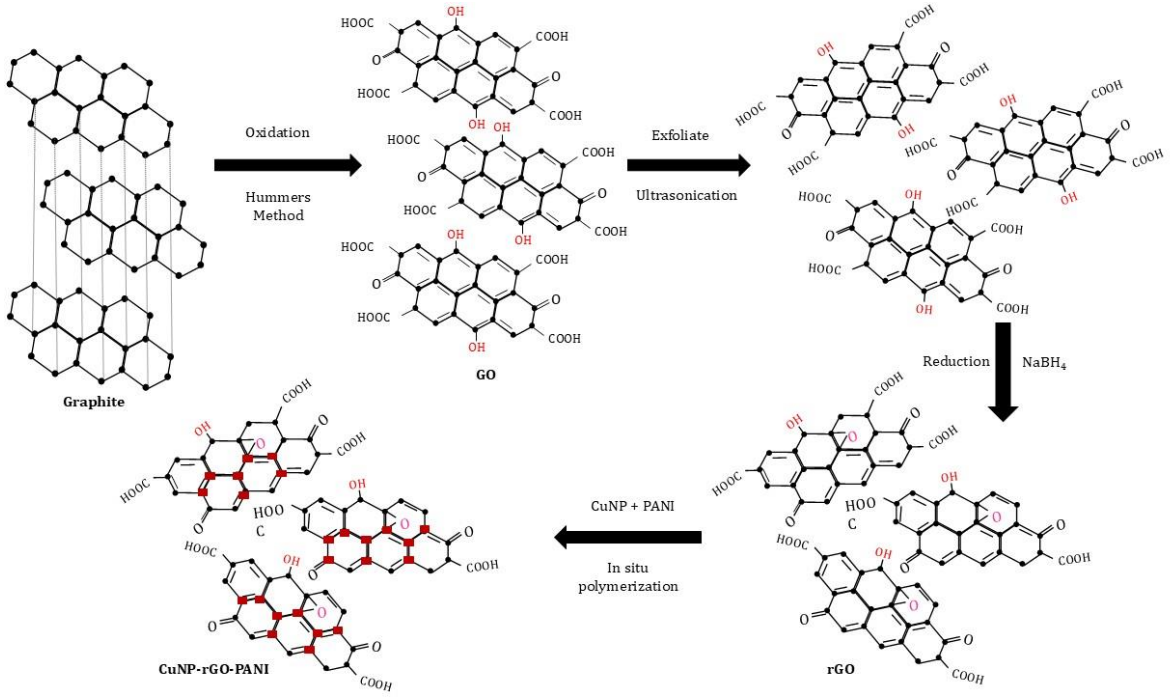

Figure 2 Synthesis process of CuNP-rGO-PANI nanocomposites

The CuNP-rGO-PANI nanocomposite, synthesized from copper nanoparticles via the chemical reduction of $CuSO_4$ using $NaBH_4$ as the reducing agent, exhibits a brownish-red colouration. This colouration indicates the successful formation of copper nanoparticles during the reduction process. Similarly, previous research has employed $NaBH_4$ as a reducing agent, synthesizing copper particles with sizes ranging from 15 to 50 nm. The brownish-red colour result is also by the studies of (Amjad et al., 2021) and (Choi, Bae and Ahn, 2016), who also employed $NaBH_4$ as the reductant. The following mechanism can elucidate the chemical reaction between $CuSO_4$ and $NaBH_4$:

$$CuSO_4 + 2NaBH_4 + 6H_2O \rightarrow Cu(s) + 2B(OH)_3 + 2NaOH + 4H_2(g) \quad (3)$$

The combination of colloidal CuNPs and rGO resulted in the deposition of copper nanoparticles on graphene sheets (red rectangles in Figure 2). Aniline functions as a stabilizing agent for the copper nanoparticles, forming an aniline-Cu complex through an in situ polymerization process. The polymerization process is indicated by a change in the colour of the mixed solution, which takes on a greenish-black hue.

To illustrate the interaction of all components in the formation of the CuNPs-rGO-PANI nanocomposite, the process begins with the reduction of graphene oxide into reduced graphene oxide (rGO) using $NaBH_4$, which leads to structural changes by removing oxygen functional groups. Next, copper nanoparticles (CuNPs) are formed through the reduction of Cu^{2+} ions, with their interaction with rGO occurring via π-π stacking or electrostatic forces. Subsequently, polyaniline (PANI) is synthesized through oxidative polymerization of aniline monomers on the rGO-CuNPs surface, where PANI interacts with CuNPs and rGO via hydrogen bonding or electrostatic attraction. Finally, the well-dispersed CuNPs on rGO, combined with the PANI matrix, create a conductive network, forming the CuNPs-rGO-PANI nanocomposite.

In the formation of CuNP-rGO-PANI nanocomposites, several crucial interactions occur among its components CuNPs, rGO, and PANI that determine the structural, morphological, and functional properties of the resulting nanocomposites. Interaction of CuNPs with rGO: CuNPs synthesized in-situ can interact with the functional oxygen groups on the surface of rGO through

electrostatic forces. Functional groups such as carbonyl (-C=O) and hydroxyl (-OH) on rGO serve as nucleation sites for CuNP growth. CuNPs can adsorb onto the surface of rGO via π-π interactions between the free electrons on Cu metal and the aromatic structure of rGO. Additionally, rGO prevents CuNP agglomeration by providing a large surface area that supports even dispersion of nanoparticles (Pegu et al., 2023).

Interaction of CuNPs with PANI: CuNPs interact with the amine (-NH) and imine (=N) groups within the PANI polymer chain. CuNPs act as doping agents for PANI, enhancing conductivity by modifying the electronic structure of the polymer. The functional groups in PANI can form complexes with copper ions during synthesis, thereby improving the stability of CuNPs. The aromatic structure of PANI enables π-π interactions with rGO, enhancing electron transfer. Amine (-NH) and hydroxyl (-OH) groups in PANI can interact with functional oxygen groups on rGO through hydrogen bonding. The combination of rGO and PANI improves the nanocomposite's conductivity, as rGO serves as a rapid electron transfer pathway, while PANI provides mechanical flexibility.

The CuNP-rGO-PANI nanocomposite is formed through a combination of electrostatic, covalent, and π-π stacking interactions among its components. The presence of rGO supports CuNP dispersibility and enhances the nanocomposite's conductivity, while PANI provides structural stability and flexibility. These synergistic interactions make CuNP-rGO-PANI a promising candidate for sensor applications and conductive inks (Pegu et al., 2023).

3.2. Raman Spectroscopy Characterisation Results

Raman spectroscopy offers insights into the extent of the reduction of rGO and the intermolecular interactions between different components (Sonawane, Mujawar and Bhansali, 2019). As illustrated in Figure 3(a), two distinct peaks are discernible at 1346.80 cm^{-1} and 1597.81 cm^{-1} wavenumbers. These are designated D (defect) and G (graphitic) peaks, respectively, and serve as carbon marker spectra in Raman spectroscopy. The characterization results indicate a ratio of 1.2 between the intensity of the ID and IG peaks. The elevated intensity of the D peak and the ID/IG ratio suggest the formation of rGO with a defective structure. The defects are primarily attributable to the chemical reduction process, which removes oxide groups, including C=O (carbonyl), O-H (hydroxyl), and C-OH (carboxyl), thereby disrupting the π-conjugated network in the graphene structure. It is also possible that some of the remaining oxide groups may contribute to the formation of structural defects (Chadha, Sharma and Saini, 2021).

As illustrated in Figure 3(b), the peaks emerge at 1340.61 cm^{-1} and 1550.27 cm^{-1}, accompanied by an augmentation in the D peak intensity, culminating in an ID/IG ratio of 1.28. The increase in the ratio from rGO (1.2) to CuNP-rGO-PANI (1.28) may indicate the presence of structural defects, which could enhance the sensor's sensitivity. If an interaction occurs between CuNPs and rGO-PANI, it suggests the potential for improved conductivity and sensing properties. This enhancement is attributed to the unique electrical characteristics of metal nanoparticles, which, when combined with conducting polymers, can significantly boost the electrochemical response and efficiency of sensors for detecting various analytes (Shen, Zhao and Wan, 2021).

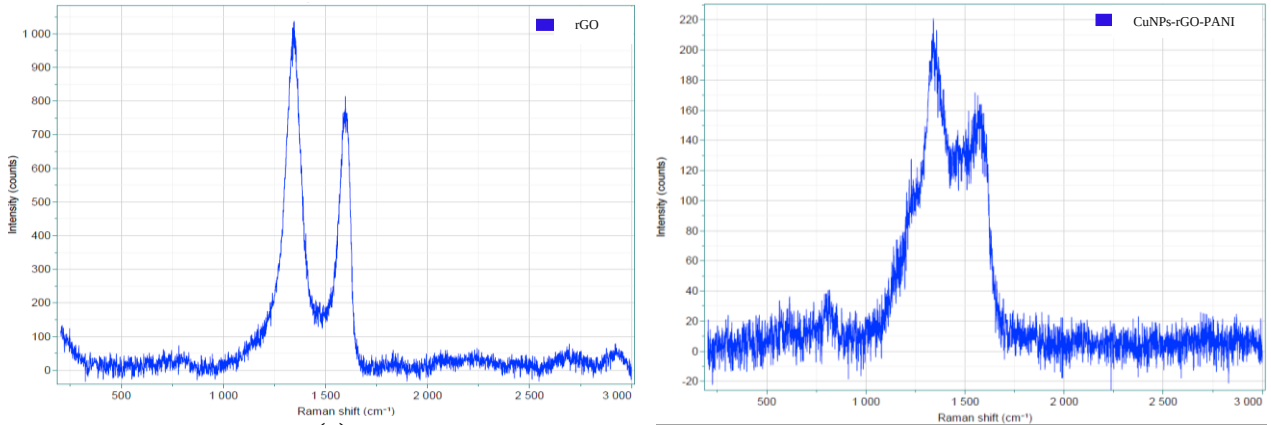

(a) (b)

Figure 3 Raman Spectroscopy characterisation results of (a) rGO, (b) CuNPs-rGO-PANI

The results of Raman spectroscopy indicate that the incorporation of copper nanoparticles (CuNPs) increases the ID/IG ratio, which indicates an enhancement in the prevalence of structural defects in rGO. This is attributed to the interaction between the nanoparticles and the rGO matrix and the thermal processes that occur during the synthesis phase. The thermal process employed during synthesizing nanocomposites also affects the structure of rGO and metal nanoparticles, thereby contributing to the observed changes in structural defects.

The significant changes in the Raman spectrum after combining rGO with PANI and Cu are caused by several key factors. The electronic interaction between rGO, PANI, and Cu alters the electron distribution, affecting the vibrational modes of carbon bonds in rGO. The presence of CuNPs also contributes through charge transfer, which can reduce the intensity of the D and G peaks in the Raman spectrum. Additionally, the structure of rGO undergoes modifications due to increased defects or disorder when integrated with PANI and Cu, potentially increasing the ID/IG ratio. The optical shielding effect of CuNPs and PANI also plays a role in reducing the Raman spectrum intensity, as both can absorb or scatter the excitation laser light (Jezzini et al., 2024; Saini et al., 2024).

3.3 SEM Characterisation Results

The surface area morphology of the graphene-based nanocomposites was examined using a SEM test. A SEM provides a relatively low-resolution overview of the composite's surface morphology, revealing the general distribution of copper nanoparticles (CuNPs), reduced graphene oxide (rGO) sheets, and polyaniline (PANI) structures (Darwish et al., 2019). Electron microscopy images were illustrate the structure of rGO as graphene sheets exfoliated by ultrasonication. Similar findings were reported by (Sharma et al., 2017) and (Gul et al., 2023), who employed the Hummers method for synthesis (Liu et al., 2014). Meanwhile, the morphology of the nanocomposites, comprising Cu and PANI particles of varying sizes and shapes dispersed and adhered to the rGO surface. Microscopic examination reveals that the particles are irregularly shaped and distributed uniformly. The presence of surface pores results in a significantly clustered mesostructure, facilitating the dispersion of metal ions into the nanocomposite matrix (Salamani et al., 2018).

A semi-quantitative calculation of particle size distribution was carried out based on the SEM image obtained, utilizing ImageJ software for image processing (Fritz et al., 2024; Sasri et al., 2018). The initial step involves calibrating the digital image by setting the appropriate scale. Next, the SEM digital images are processed using the Threshold function to enhance the distinction between the object and its background. The analysis is then performed using Analyze > Analyze Particles, which provides data on the total area of all identified particles. Assuming the particles are spherical, their

diameters can be estimated based on the calculated average area. The particle size distribution was calculated using the ImageJ software, as illustrated in the following example:

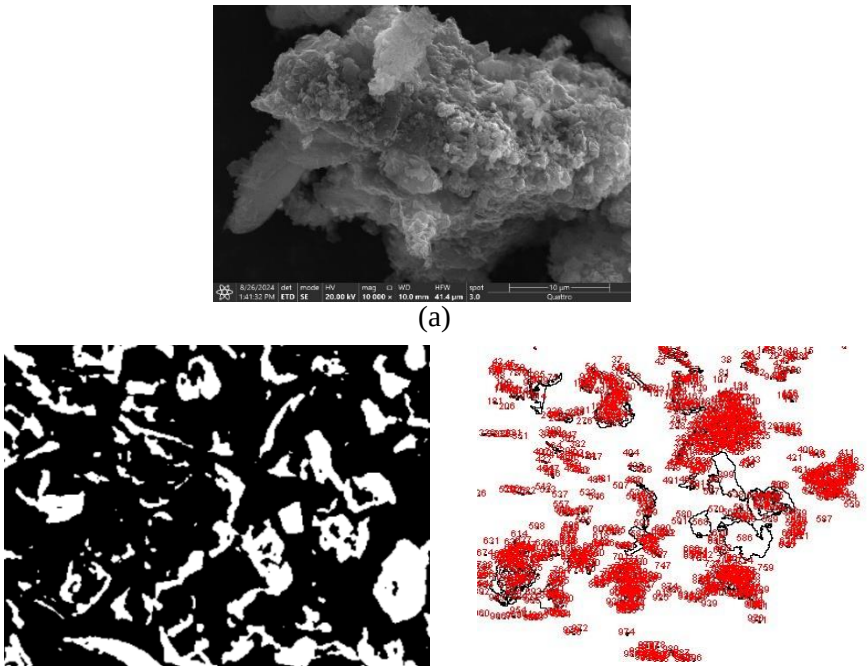

Figure 4 a. SEM characterisation results of CuNP-GO-PANI at ×20000 magnification, b. Treshold results of CuNP-rGO-PANI in ImageJ software, c. Outline results of CuNP-rGO-PANI in ImageJ software

Figure 4 illustrates the outcomes of image processing conducted with the ImageJ software, which was employed to ascertain the particle size distribution. The results of SEM images of CuNP-rGO-PANI nanocomposites that have undergone image calibration are presented in Figure 4a. The threshold results, which differentiate the object in question from the background (Figure 4b), are presented herewith. Figure 4c illustrates the outline results, which display the area data that has been defined. The particle size distribution is presented in the following section, with the data obtained through ImageJ software:

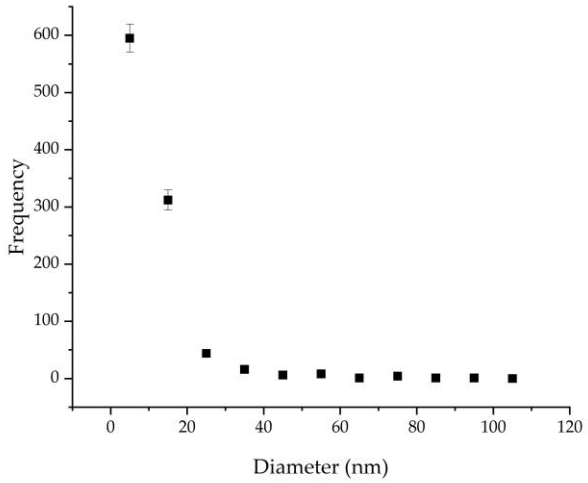

Figure 5 Particle size distribution of nanocomposites CuNP-rGO-PANI using ImageJ software

Table 1 Particle size calculation results

Nanocomposites	Average area (nm^2)	Mean Diameter (nm)	Smallest diameter (nm)	Largest diameter (nm)
CuNP-rGO-PANI	667.23	11.48	7.67	99.68

Table 1 presents the particle size distribution obtained through image analysis using the ImageJ software. The CuNP-rGO-PANI nanocomposite particles exhibit an average diameter of 11.48 nm, ranging from 7.67 to 99.68 nm. This is consistent with the typical nanoscale range of 1-100 nm, as previously reported by (Mekuye & Abera, 2023; Joudeh & Linke, 2022) In conclusion, the SEM analysis provided a comprehensive representation of the morphology and particle size distribution, indicating that the synthesis method employed effectively yielded nanocomposites with an optimal nano-size and considerable potential for RFID chipless sensor applications.

3.4. FTIR Spectrophotometer Characterisation Results

FTIR spectroscopy was employed to ascertain the chemical functionalities formed in the CuNP-rGO-PANI nanocomposites (Valan et al., 2022). This analysis is based on detecting transmittance peaks in infrared spectra associated with specific chemical bond vibrations in the material. By analyzing these spectra, it is possible to identify the functional groups that have been formed and establish a link between them and the material's structure. FTIR is a widely employed method for elucidating the chemical alterations and interactions occurring between the constituents of a nanocomposite.

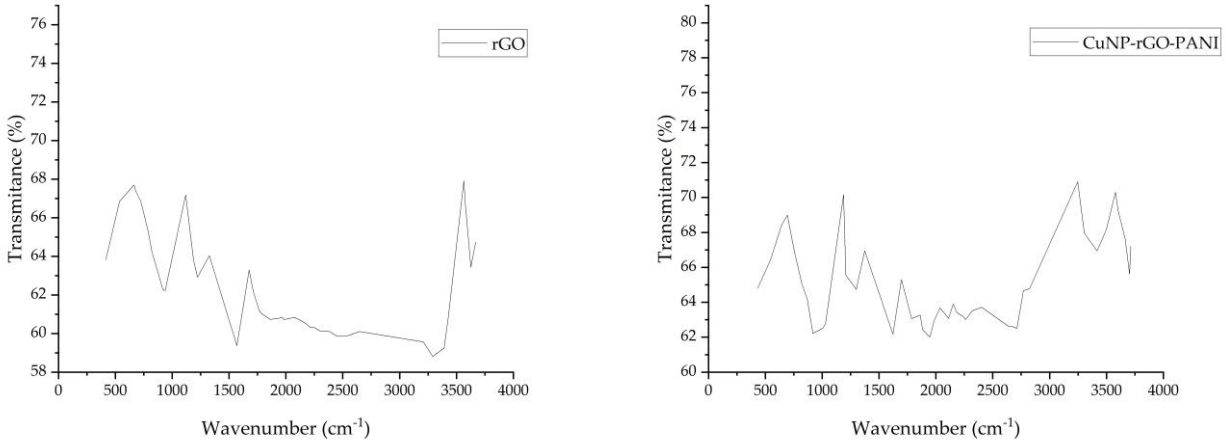

Figure 6 The FTIR characterisation results of (a) rGO, (c) CuNP-rGO-PANI

Figure 6(a) illustrates the FTIR characterization results of rGO, which reveal the presence of the leading functional group of rGO, C=C, at a wavenumber of 1569.76 cm^{-1}. This peak is typically associated with sp^2 hybridized carbon atoms and C-C stretching vibrations within the graphene lattice. This peak indicates the presence of conjugated double bonds, which constitute the backbone of the rGO structure. During the reduction process, many oxygen groups are removed. The C=C functional group represents the fundamental structure of rGO, comprising hexagonal carbon double bonds. It contributes to the material's strength and electrical conductivity due to its high bond energy. These findings are consistent with those reported by (Gul et al., 2023; Mallakpour & Hussain, 2021; Kumar et al., 2018) on rGO and graphene materials. Additionally, another absorption peak appears at 3579 cm^{-1}, indicating the presence of an O-H functional group, which suggests the presence of water in the compound.

The FTIR characterization of the CuNP-rGO-PANI nanocomposite revealed an absorption peak at 1300.02 cm^{-1} (Figure 6(b)). The observed peak indicates the presence of C-O bonds derived from carboxyl or phenolic groups in rGO that interact with PANI. Furthermore, it suggests the existence of interactions or binding between polyaniline and rGO, as well as between rGO and CuNP. Furthermore, an additional absorption peak was identified at 1622.49 cm^{-1}, frequently associated with C-C vibrations. This suggests the presence of an aromatic structure in PANI. This results in the polyaniline structure being retained in the composite, with interactions that affect the electronic structure of polyaniline, though not to the extent of destruction. Furthermore, the incorporation of CuNPs has been observed to affect the oxidation state of PANI and the reduction of graphene oxide, which in turn gives rise to changes in peak intensity and position in the FTIR spectrum (Singh et al., 2022). Another absorption peak appears at 3416 cm^{-1}, indicating the presence of the N-H group in aniline.

3.5. Conductive Ink Formulation and Sensor Printing Results

The results of the sensor printing process, conducted using the screen printing method, yielded three sensors with distinct substrate types. Table 2 illustrates the thickness of each sensor after the curing process.

Table 2 Sensor printing results based on the substrate used

Substrate	Flat thickness(mm)
PET	0.27
Glass	0.31
Photo paper	0.19

The thickness of the sensor layer on PET plastic, photo paper, and glass substrates exhibits notable discrepancies that influence the functionality of CuNP-rGO-PANI-based conductive ink sensors. The distinctive attributes of each substrate influence the flexibility, mechanical resistance, and sensitivity of the sensors, which are essential for their functionality. After curing on PET plastic substrates, the ink layer thickness is 0.27 mm, providing an optimal balance between flexibility and mechanical resistance, which is crucial for applications where durability is a prerequisite (Lepak-Kuc et al., 2022). On photo paper, the ink layer is of a lesser thickness, measuring approximately 0.19 mm after curing. This increases sensitivity but reduces mechanical resistance, which renders the sensor more susceptible to damage (Brathwaite et al., 2023).

In contrast, the ink is less likely to permeate on glass, resulting in a thicker layer (approximately 0.31 mm after curing), which offers enhanced structural stability but may compromise flexibility, which is critical for specific applications (Yi, Samara and Wang, 2021). The coating thickness generally depends on the substrate type and the moulding technique employed. While thinner layers enhance sensitivity, they may diminish durability, underscoring a trade-off in sensor design based on substrate selection. Conversely, a thicker coating on a more rigid substrate may enhance stability but may constrain flexibility, underscoring the necessity for meticulous deliberation in sensor applications.

3.6. Sensor Electrical Conductivity Measurement Results

Direct current conductivity measurements measure the overall electrical conductivity of the nanocomposite. This measurement indicates the ease with which charge carriers can traverse the material under a constant electric field. The sensor's electrical conductivity was determined by applying the four-point probe method, with the resulting data subsequently calculated in

accordance with the Smits equation (Istuk et al., 2023). Table 3 presents the parameters of the sensor electrical conductivity measurement results.

Table 3 Measurement results of resistivity and electrical conductivity of the sensor

Substrate	Resistivity (Ωcm)	Electrical conductivity (S/cm)
PET	673.14 x 10^{-3}	1.49
Glass	821.52 x 10^{-3}	1.22
Photo paper	943.75 x 10^{-3}	1.06

The conductivity of the CuNP-rGO-PANI-based conductive ink sensor is significantly affected by the thickness of the ink layer, the distribution of conductive particles (CuNP and rGO), and the substrate utilized. The resistivity of the CuNP-rGO-PANI-based conductive ink sensor on a PET plastic substrate is lower (673.14 x 10^{-3} Ωcm), which is inversely proportional to the higher electrical conductivity of 1.486 S/cm. This is due to the optimal ink layer thickness and relatively smooth surface of PET, allowing for a more even distribution of CuNP and rGO nanoparticles, forming effective conduction pathways and enhancing electron transport (Henley et al., 2015). On photo paper, despite the thinner ink layer, the ink's uneven distribution and the paper's absorbent nature result in an increased resistivity (943.75 x 10^{-3} Ωcm), which in turn leads to a reduction in conductivity. Conversely, glass substrates exhibit a lower conductivity of 1.0596 S/cm compared to PET due to the greater thickness of the ink layer, which impedes electron transport. However, glass displays superior structural stability (Henley et al., 2015). PET generally provides optimal conductivity, while photographic paper and glass exhibit decreased conductivity due to suboptimal coating thickness and uneven particle distribution.

The resistivity value is calculated based on the thickness measurement of the printed pattern on the substrate. The sensor, printed on photo paper, exhibited a high resistivity value of 943.75 x 10^{-3}. The resistivity value obtained on photo paper is superior to that obtained on glass and PET substrates. It has been demonstrated in multiple studies that glossy photo paper (Epson) contains a surface coated with chloride ions. These ions migrate to the copper film during copper dispersion deposition and fluid vehicle absorption, promoting the decapsulation of copper nanoparticles from the deagglomeration agent and assisting the sintering process (Vaseem et al., 2016; Magdassi et al., 2010). The resistivity values on PET substrates are superior to those printed on other substrates, as a lower resistivity of an ink correlates with enhanced conductivity (Fernandes et al., 2020; Magdassi et al., 2010). Nevertheless, the relatively low resistivity value can be attributed to the higher copper nanoparticle content (30 wt%) employed.

4. Conclusions

CuNP-rGO-PANI nanocomposites have demonstrated considerable potential for use in various printed sensor applications. The structure and characteristics of the nanocomposite materials are significantly influenced by including copper nanoparticles. The Raman spectroscopy results demonstrated that incorporating Cu nanoparticles elevated the ID/IG ratio, indicating an augmentation in structural defects in rGO due to the interaction between nanoparticles and the rGO matrix and thermal processes that occurred during synthesis. The particle size of the CuNP-rGO-PANI nanocomposite was determined to be 11.48 nm on average through SEM analysis. FTIR characterization demonstrated the interaction between polyaniline (PANI), reduced graphene oxide (rGO), and copper nanoparticles (CuNP), which affected the electronic structure of PANI without significantly damaging it. Furthermore, the addition of CuNPs alters the oxidation state of PANI and reduces graphene oxide, as evidenced by shifts in the intensity and position of the FTIR peaks. The

conductivity of the CuNP-rGO-PANI-based conductive ink sensor is contingent upon the thickness of the ink layer, the distribution of conductive particles, and the type of substrate utilized. The PET plastic substrate exhibited the highest conductivity of 1.486 S/cm, attributed to the optimal coating thickness and uniform particle distribution. In contrast, the photographic paper and glass substrates demonstrated lower conductivity, which can be attributed to suboptimal coating thickness and an uneven particle distribution. The sensor's conductivity is primarily determined by the thickness of the ink layer and the substrate's surface properties.

Acknowledgements

The author would like to thank the following institutions for granting this doctoral scholarship at BPI (Beasiswa Pendidikan Indonesia) with the ID number 202101122325, and for supporting this research: (1) Pusat Pembiayaan dan Asesmen Pendidikan Tinggi (Center for Higher Education Funding and Assessment)-PPAPT Ministry of Higher Education, Science, and Technology of Republic Indonesia, and (2) Lembaga Pengelola Dana Pendidikan (Education Fund Management Institution)-LPDP, Ministry of Finance Indonesia. Fund Project Number: 1985/J5.2.3./BPI.06/10/2021.

Author Contributions

Priska Wisudawaty: Writing-original draft, review & editing. Endang Warsiki: Review, editing, and supervision. Sugiarto: Review and supervision. Taufik Djatna: Review, editing, and supervision.

Conflict of Interest

The authors declare no conflicts of interest.

References

Amjad, R., Mubeen, B., Ali, S.S., Imam, S.S., Alshehri, S., Ghoneim, M.M., Alzarea, S.I., Rasool, R., Ullah, I., Nadeem, M.S. and Kazmi, I., 2021, 'Green synthesis and characterization of copper nanoparticles using fortunella margarita leaves', *Polymers*, vol. 13 no. 24, pp. 1–12, https://doi.org/10.3390/polym13244364

Bhangoji, J.C., Sahoo, S., Satpati, A.K. and Shendage, S.S., 2021, 'Facile and green synthesis of silver nanoparticle-reduced graphene oxide composite and its application as nonenzymatic electrochemical sensor for hydrogen peroxide', *Current Chemistry Letters*, vol. 10, no. 3, pp. 295–308, https://doi.org/10.5267/J.CCL.2021.3.002

Brathwaite, K.G., Wyatt, Q.K., Atassi, A., Gregory, S.A., Throm, E., Stalla, D., Yee, S.K., Losego, M.D. and Young, M.J., 2023, 'Effects of film thickness on electrochemical properties of nanoscale polyethylenedioxythiophene (PEDOT) thin films grown by oxidative molecular layer deposition (oMLD)', *Nanoscale*, vol. 15, no. 13, pp. 6187–6200, https://doi.org/10.1039/d3nr00708a

Chadha, N., Sharma, R. and Saini, P., 2021, 'A new insight into the structural modulation of graphene oxide upon chemical reduction probed by Raman spectroscopy and X-ray diffraction', *Carbon Letters*, vol 31, no. 6, pp. 1125–1131, https://doi.org/10.1007/s42823-021-00234-5

Choi, M.W., Bae, M.H. and Ahn, J.-H., 2016, 'Synthesis of Copper Nanoparticles by a Chemical Reduction Method', *Journal of Korean Powder Metallurgy Institute*, vol. 23, no. 3, pp. 228–234, https://doi.org/10.4150/kpmi.2016.23.3.228

Darwish, A.G., Ghoneim, A.M., Hassaan, M.Y., Shehata, O.S. and Turky, G.M., 2019, 'Synthesis and characterization of polyaniline/Mn3O4/Reduced graphene oxide nanocomposite', *Egyptian Journal of Chemistry*, vol. 62, pp. 251–265. https://doi.org/10.21608/ejchem.2019.13194.1821

Dobrovolný, K., Ulbrich, P. and Bartůněk, V., 2016, 'Synthesis of Ultrafine Metallic Copper Nanocubes Using Ethanol-Ionic Liquid Approach', *Journal of Cluster Science*, vol. 27, no. 6, pp. 1843–1847, https://doi.org/10.1007/s10876-016-1065-0

Fajarani, R., Rahman, S.F., Pangesty, A.I., Katili, P.A., Park, D.H. and Basari, 2024, 'Physical and Chemical Characterization of Collagen/Alginate/Poly(Vinyl Alcohol) Scaffold with the Addition of Multi-Walled Carbon Nanotube, Reduced Graphene Oxide, Titanium Dioxide, and Zinc Oxide Materials', *International Journal of Technology*, vol. 15, no. 2, pp. 332–341, https://doi.org/10.14716/ijtech.v15i2.6693

Fernandes, I.J., Aroche, A.F., Schuck, A., Lamberty, P., Peter, C.R., Hasenkamp, W. and Rocha, T.L.A.C., 2020, 'Silver nanoparticle conductive inks: synthesis, characterization, and fabrication of inkjet-printed flexible electrodes', *Scientific Reports*, vol. 10, no. 1, pp. 1–11. https://doi.org/10.1038/s41598-020-65698-3

Filip, J., Kasák, P. and Tkac, J., 2015, 'Graphene as signal amplifier for preparation of ultrasensitive electrochemical biosensors', *Chemical Papers*, vol. 69, no. 1, pp. 112–133, https://doi.org/10.1515/chempap-2015-0051

Fritz, M., Deutsch, L.F., Wijaya, K.P., Götz, T. and Fischer, C.B., 2024, 'An Image-Processing Tool for Size and Shape Analysis of Manufactured Irregular Polyethylene Microparticles', *Microplastics*, vol. 3, no. 1, pp. 124–146, https://doi.org/10.3390/microplastics3010008

Gao, Y., 2017, 'Graphene and polymer composites for supercapacitor applications: A review', *Nanoscale Research Letters*, vol. 12, no. 1, https://doi.org/10.1186/s11671-017-2150-5

Gul, W., Akbar Shah, S.R., Khan, A., Ahmad, N., Ahmed, S., Ain, N., Mehmood, A., Salah, B., Ullah, S.S. and Khan, R., 2023, 'Synthesis of graphene oxide (GO) and reduced graphene oxide (rGO) and their application as nano-fillers to improve the physical and mechanical properties of medium density fiberboard', *Frontiers in Materials*, vol. 10, pp. 1–10, https://doi.org/10.3389/fmats.2023.1206918

Hardi, G.W. and Rahman, S.F., 2020, 'Amperometric Detection of Dopamine based on a Graphene Oxide/PEDOT:PSS Composite Electrode', *International Journal of Technology*, vol. 11, no. 5, pp. 974–983. https://doi.org/10.14716/ijtech.v11i5.4323

Henley, S.J., Kula, M., Brunton, A.N., Chan, C.W.A., Dixon, R. and Dunne, B., 2015, 'Low-cost copper conductive grids for thin-film solar cells formed by screen printing and laser sintering', *2015 IEEE 42nd Photovoltaic Specialist Conference, PVSC 2015*, pp. 2–4, https://doi.org/10.1109/PVSC.2015.7356285

Istuk, N., Benchakroun, H., Elahi, A., O'halloran, M., Matta, R., Moreau, D., O'connor, R. and Dunne, E., 2023, 'Reducing Sensing Volume Confounding Effects in Conductivity Measurements: The Use of a Miniaturised Four-Electrode Probe', *ICECOM 2023 - 24th International Conference on Applied Electromagnetics and Communications*, C(July), https://doi.org/10.1109/ICECOM58258.2023.10367941

Joudeh, N. and Linke, D., 2022, 'Nanoparticle classification, physicochemical properties, characterization, and applications: a comprehensive review for biologists', *Journal of Nanobiotechnology*, vol. 20, no. 1, pp. 1–29. https://doi.org/10.1186/s12951-022-01477-8

Jezzini, A., Davidson, A., Hamieh, T. and Toufaily, J., 2024, 'Exploring Reduced Graphene Oxide Sheets Stabilized by Cu(II) and Cu(I) Cations in Ethanol', *Crystals*, vol. 14, no. 7, pp.1–16, https://doi.org/10.3390/cryst14070654

Junervin, Djatna, T. and Fahma, F., 2020, 'A synthesis of AgNP-rGO-PANI nanocomposite and its use in fabrication of chipless RFID sensor: Current research progress', *IOP Conference Series: Earth and Environmental Science*, vol. 472, no. 1, https://doi.org/10.1088/1755-1315/472/1/012027

Kalambate, P.K., Dar, R.A., Karna, S.P. and Srivastava, A.K., 2015, 'High performance supercapacitor based on graphene-silver nanoparticles-polypyrrole nanocomposite coated on glassy carbon electrode', *Journal of Power Sources*, vol. 276, pp. 262–270, https://doi.org/10.1016/j.jpowsour.2014.11.130

Kumar, V., Gupta, R.K., Gundampati, R.K., Singh, D.K., Mohan, S., Hasan, S.H. and Malviya, M., 2018, 'Enhanced electron transfer mediated detection of hydrogen peroxide using a silver nanoparticle-reduced graphene oxide-polyaniline fabricated electrochemical sensor', *RSC Advances*, [online] vol. 8, no. 2, pp. 619–631, https://doi.org/10.1039/c7ra11466d

Kusrini, E., Suhrowati, A., Usman, A., Khalil, M. and Degirmenci, V., 2019, 'Synthesis and characterization of graphite oxide, graphene oxide, and reduced graphene oxide from graphite waste using modified hummers' method and zinc as reducing agent, *International Journal of Technology*, vol. 10, no. 6, pp. 1093–1104, https://doi.org/10.14716/ijtech.v10i6.3639

Lepak-Kuc, S., Wasilewska, K., Janczak, D., Nowicka, T. and Jakubowska, M., 2022, 'Conductive Layers on a Shrinkable PET Film by Flexographic Printing', *Materials*, vol. 15, no. 10,

https://doi.org/10.3390/ma15103649

Li, B.Q., Nie, F., Sheng, Q.L. and Zheng, J. Bin, 2015, 'An electrochemical sensor for sensitive determination of nitrites based on Ag-Fe3O4-graphene oxide magnetic nanocomposites', *Chemical Papers*, vol. 69, no. 7, pp. 911–920. https://doi.org/10.1515/chempap-2015-0099

Li, R., Yang, T., Li, Z., Gu, Z., Wang, G. and Liu, J., 2017, 'Synthesis of palladium@gold nanoalloys/nitrogen and sulphur-functionalized multiple graphene aerogel for electrochemical detection of dopamine', *Analytica Chimica Acta*, [online] 954, pp. 43–51, https://doi.org/10.1016/j.aca.2016.12.031

Li, Z.F., Zhang, H., Liu, Q., Liu, Y., Stanciu, L. and Xie, J., 2014, 'Covalently-grafted polyaniline on graphene oxide sheets for high performance electrochemical supercapacitors', *Carbon*, [online] vol. 71, pp. 257–267, https://doi.org/10.1016/j.carbon.2014.01.037

Liu, L., Shen, Z., Zhang, X. and Ma, H., 2021, 'Highly conductive graphene/carbon black screen printing inks for flexible electronics', *Journal of Colloid and Interface Science*, [online] vol. 582, pp. 12–21. https://doi.org/10.1016/j.jcis.2020.07.106

Liu, Y., Li, Q., Feng, Y.Y., Ji, G.S., Li, T.C., Tu, J. and Gu, X.D., 2014, 'Immobilisation of acid pectinase on graphene oxide nanosheets', *Chemical Papers*, vol. 68, no. 6, pp. 732–738, https://doi.org/10.2478/s11696-013-0510-x

Magdassi, S., Grouchko, M., Berezin, O. and Kamyshny, A., 2010, 'Triggering the sintering of silver nanoparticles at room temperature', *ACS Nano*, vol. 4, no. 4, pp. 1943–1948, https://doi.org/10.1021/nn901868t

Mallakpour, S. and Hussain, C.M., 2021, *'Handbook of Consumer Nanoproducts', Handbook of Consumer Nanoproducts*, https://doi.org/10.1007/978-981-15-6453-6

Martinez-Lombardia, E., Gonzalez-Garcia, Y., Lapeire, L., De Graeve, I., Verbeken, K., Kestens, L., Mol, J.M.C. and Terryn, H., 2014, 'Scanning electrochemical microscopy to study the effect of crystallographic orientation on the electrochemical activity of pure copper', *Electrochimica Acta*, [online] vol. 116, pp. 89–96, https://doi.org/10.1016/j.electacta.2013.11.048

Mekuye, B. and Abera, B., 2023, 'Nanomaterials: An overview of synthesis, classification, characterization, and applications', *Nano Select*, vol. 4, no. 8, pp. 486–501, https://doi.org/10.1002/nano.202300038

Mohanapriya, K., Ghosh, G. and Jha, N., 2016, 'Solar light reduced Graphene as high energy density supercapacitor and capacitive deionization electrode', *Electrochimica Acta*, [online] vol. 209, pp. 719–729, https://doi.org/10.1016/j.electacta.2016.03.111

Mooss, V.A., Bhopale, A.A., Deshpande, P.P. and Athawale, A.A., 2017, 'Graphene oxide-modified polyaniline pigment for epoxy based anti-corrosion coatings', *Chemical Papers*, vol. 71, no. 8, pp. 1515–1528, https://doi.org/10.1007/s11696-017-0146-3

Mousavi-Kamazani, M., Zarghami, Z. and Salavati-Niasari, M., 2016, 'Facile and Novel Chemical Synthesis, Characterization, and Formation Mechanism of Copper Sulfide (Cu2S, Cu2S/CuS, CuS) Nanostructures for Increasing the Efficiency of Solar Cells', *Journal of Physical Chemistry C*, vol. 120, no. 4, pp. 2096–2108, https://doi.org/10.1021/acs.jpcc.5b11566

Murdiya, F., Hendri, Y.B., Hamzah, A., Frimayanti, N. and Amri, A., 2022, 'Few-Layer Wrinkled Graphene (FLwG) Obtained from Coconut-Shell-Based Charcoal using a High-Voltage Plasma Method', *International Journal of Technology*, vol. 13, no. 1, pp. 157–167, https://doi.org/10.14716/ijtech.v13i1.4572

Nugrahaningtyas, K.D., Kusrini, E., Salsabila, S., Fitriana, D. and Usman, A., 2025, 'Synthesis of Transition Metal-Nanochitosan Composites Using Ni , Cu , Zn , and Ag Metal Ions and Applications as Antibacterial Agents', *International Journal of Technology* , vol. 16, no. 624, pp. 207–220, https://doi.org/10.14716/ijtech.v16i1.6969

Nur, H.M., Song, J.H., Evans, J.R.G. and Edirisinghe, M.J., 2002, 'Ink-jet printing of gold conductive tracks', *Journal of Materials Science: Materials in Electronics*, vol. 13, no. 4, pp. 213–219, https://doi.org/10.1023/A:1014827900606

Pandey, A. and Qureshi, A., 2017, 'Surface modified graphene oxide nanosheets by gold ion implantation as a substrate for surface enhanced Raman scattering', *Journal of Alloys and Compounds*, [online] vol. 703, pp. 500–507, https://doi.org/10.1016/j.jallcom.2017.02.020

Park, B.K., Kim, D., Jeong, S., Moon, J. and Kim, J.S., 2007, 'Direct writing of copper conductive patterns

583 by ink-jet printing', *Thin Solid Films*, vol. 515, (19 SPEC. ISS.), pp. 7706–7711,
584 https://doi.org/10.1016/j.tsf.2006.11.142
585 Pegu, B., Konwar M., Sarma, D., Konwer, S., 2024, 'Cu nanoparticle anchored highly conducting, reusable
586 multifunctional rGO/PANI nanocomposite: A novel material for methanol sensor and a catalyst for click
587 reaction', *Synthetic Metals*, vol. 301, https://doi.org/10.1016/j.synthmet.2023.117516
588 Petrovski, A., Paunović, P., Avolio, R., Errico, M.E., Cocca, M., Gentile, G., Grozdanov, A., Avella, M.,
589 Barton, J. and Dimitrov, A., 2017, 'Synthesis and characterization of nanocomposites based on PANI and
590 carbon nanostructures prepared by electropolymerization', *Materials Chemistry and Physics*, vol. 185, pp. 83–
591 90. https://doi.org/10.1016/j.matchemphys.2016.10.008
592 Qiu, Z., He, D., Wang, Y., Zhao, X., Zhao, W. and Wu, H., 2017, 'High performance asymmetric
593 supercapacitors with ultrahigh energy density based on hierarchical carbon nanotubes@NiO core-shell
594 nanosheets and defect-introduced graphene sheets with hole structure', *RSC Advances*, vol. 7, no. 13, pp. 7843–
595 7856, https://doi.org/10.1039/c6ra27369f
596 Reddy, B.N., Pathania, A., Rana, S., Srivastava, A.K. and Deepa, M., 2014, 'Plasmonic and conductive Cu
597 fibers in poly (3,4-ethylenedioxythiophene)/Cu hybrid films: Enhanced electroactivity and electrochromism',
598 *Solar Energy Materials and Solar Cells*, vol. 121, pp. 69–79, https://doi.org/10.1016/j.solmat.2013.10.027
599 Saini, A., Madhuri, A., Sahoo, S.K., Devi, P.S., Jena, S., Laha, S. and Swain, B.P., 2024, 'Investigation of
600 microstructural, chemical bonding and optical properties of Fe-Cu/rGO nanocomposites', *Journal of Alloys and
601 Metallurgical Systems*, [online] 5(December 2023), p.100053, https://doi.org/10.1016/j.jalmes.2023.100053
602 Salamani, A., Merrouche, A., Telli, L., Gómez-Romero, P. and Huertas, Z.C., 2018, 'Synthesis and
603 Caracterization of Mesoporous FePO4 as Positive Electrode Materials for Lithium Batteries', *Surface
604 Engineering and Applied Electrochemistry*, vol. 54, no. 1, pp. 55–63, https://doi.org/10.3103/S106837551801012X
605 Sasri, R., Nurlina, Destiarti, L. and Syahbanu, I., 2018, 'Size analysis of silica particles extracted from solid
606 rocks from Ketapang Regency, West Kalimantan., Indonesian', *Journal of Pure and Applied Chemistry*, [online]
607 vol. 1, no. 1, pp. 39–43, https://doi.org/10.26418/indonesian.v1i1.26042
608 Shahriary, L., Nair, R., Sabharwal, S. and Athawale, A.A., 2015, 'One-step synthesis of Ag-reduced
609 graphene oxide-multiwalled carbon nanotubes for enhanced antibacterial activities', *New Journal of Chemistry*,
610 vol. 39, no. 6, pp.4583–4590. https://doi.org/10.1039/c4nj02275k
611 Sharma, V., Jain, Y., Kumari, M., Gupta, R., Sharma, S.K. and Sachdev, K., 2017, 'Synthesis and
612 Characterization of Graphene Oxide (GO) and Reduced Graphene Oxide (rGO) for Gas Sensing Application',
613 *Macromolecular Symposia*, vol. 376, no. 1, pp. 1–5, https://doi.org/10.1002/masy.201700006
614 Shen, X., Zhao, S. and Wan, A., 2021, 'A sensitive and flexible sensor enhanced by constructing graphene-
615 based polyaniline conductive networks', *Sensors and Actuators, A: Physical*, [online] vol 330, p. 112862,
616 https://doi.org/10.1016/j.sna.2021.112862
617 Shishir, M.K.H., Afrin, S., Sachchu, M.M.H., Eva, T.N., Tabassum, S., Ahmed, S., Sadia, S.I. and Alam,
618 M.A., 2024, 'Crystalline Copper Nanomaterials for Advanced Ceramic: A Comprehensive Review for
619 Functional Ceramic Coating Approaches', *Asian Journal of Advanced Research and Reports*, vol. 18, no. 8, pp. 13–
620 34, https://doi.org/10.9734/ajarr/2024/v18i8706
621 Singh, W.I., Sinha, S., Devi, N.A., Nongthombam, S., Laha, S. and Swain, B.P., 2022, 'Fabrication and
622 Characterization of Reduced Graphene Oxide/Polyaniline/Poly(Caprolactone) Electrospun Nanofiber',
623 *Arabian Journal for Science and Engineering*, [online] vol. 47, no. 1, pp. 925–934, https://doi.org/10.1007/s13369-
624 021-05901-3
625 Sonawane, A., Mujawar, M.A. and Bhansali, S., 2019, 'Atmospheric Plasma Treatment Enhances the
626 Biosensing Properties of Graphene Oxide-Silver Nanoparticle Composite', *Journal of The Electrochemical Society*,
627 vol. 166, no. 9, pp. B3084–B3090, https://doi.org/10.1149/2.0161909jes
628 Tien, H.W., Huang, Y.L., Yang, S.Y., Wang, J.Y. and Ma, C.C.M., 2011, 'The production of graphene
629 nanosheets decorated with silver nanoparticles for use in transparent, conductive films', *Carbon*, [online] vol.
630 49, no. 5, pp. 1550–1560, https://doi.org/10.1016/j.carbon.2010.12.022
631 Trisnadewi, T., Kusrini, E., Nurjaya, D.M., Paul, B., Thierry, M. and Putra, N., 2023, 'Comparison of Phase
632 Change Materials of Modified Soy Wax using Graphene and MAXene for Thermal Energy Storage Materials
633 in Buildings', *International Journal of Technology*, vol. 14, no. 3, pp. 596–605,

https://doi.org/10.14716/ijtech.v14i3.6092

Valan, S.L., De Cruz, A.E., Jacob, P.J. and Djearamane, S., 2022, 'Sustainable Synthesis of Copper Oxide Nanoparticles Using Aquilaria Malaccensis (Agarwood) Leaf Extract as Reducing Agent', *International Journal of Technology*, vol. 13, no. 5, pp. 1115–1125, https://doi.org/10.14716/ijtech.v13i5.5845

Vaseem, M., McKerricher, G. and Shamim, A., 2016, 'Robust Design of a Particle-Free Silver-Organo-Complex Ink with High Conductivity and Inkjet Stability for Flexible Electronics', *ACS Applied Materials and Interfaces*, vol. 8, no. 1, pp. 177–186, https://doi.org/10.1021/acsami.5b08125

Wang, Q., Yan, J. and Fan, Z., 2016, 'Carbon materials for high volumetric performance supercapacitors: Design, progress, challenges and opportunities', *Energy and Environmental Science*, [online] vol. 9, no. 3, pp. 729–762, https://doi.org/10.1039/c5ee03109e

Warsiki, E., 2018, 'Application of chitosan as biomaterial for active packaging of ethylene absorber', *IOP Conference Series: Earth and Environmental Science*, vol. 141, no. 1, https://doi.org/10.1088/1755-1315/141/1/012036

Wisudawaty, P., Djatna, T. and Sugiarto, 2024, 'Analysis and design of smart food packaging monitoring model based on chipless RFID sensor', *IOP Conference Series: Earth and Environmental Science*, vol. 1358, no. 1, https://doi.org/10.1088/1755-1315/1358/1/012038

Wu, L., Hao, L., Pang, B., Wang, G., Zhang, Y. and Li, X., 2017, 'MnO2 nanoflowers and polyaniline nanoribbons grown on hybrid graphene/Ni 3D scaffolds by in situ electrochemical techniques for high-performance asymmetric supercapacitors', *Journal of Materials Chemistry A*, vol. 5, no. 9, pp. 4629–4637, https://doi.org/10.1039/c6ta10757e

Xu, Q., Gu, S.X., Jin, L., Zhou, Y.E., Yang, Z., Wang, W. and Hu, X., 2014, 'Graphene/polyaniline/gold nanoparticles nanocomposite for the direct electron transfer of glucose oxidase and glucose biosensing', Sensors and Actuators', *B: Chemical*, vol. 190, pp. 562–569, https://doi.org/10.1016/j.snb.2013.09.049

Yao, Y., 2022, 'Facile Synthesis of Copper-Coated-Reduced-Graphene-Oxide and Its Application as a Highly Sensitive Electrochemical Sensor for Hydroquinone', *Journal of Chemistry*, 2022. https://doi.org/10.1155/2022/6894049

Yi, Y., Samara, A. and Wang, B., 2021, 'A new approach for an ultra-thin piezoresistive sensor based on solidified carbon ink film', *Journal of Materials Science*, vol. 56, no. 1, pp. 607–614, https://doi.org/10.1007/s10853-020-05309-8